PHYSICAL REVIEW A VOLUME 21, NUMBER 1 JANUARY 1980

Quantitative analysis of nuclear K-x-ray satellites for $Z = 50$–83

J. Smolorz, S. Hoppenau, S. Röhl, W. A. Schönfeldt, and M. Dost
Institut für Kernphysik, Universität Köln, D-5000 Köln, West Germany
(Received 30 April 1979)

K-x-ray nuclear-satellite cross sections are reported for $^{120}_{50}$Sn, $^{165}_{67}$Ho, $^{169}_{69}$Tm, $^{181}_{73}$Ta, $^{197}_{79}$Au, $^{208}_{82}$Pb, and $^{209}_{83}$Bi bombarded with 17.5–22.5-MeV α particles. Depending on target and energy, between 19 and 92% of these cross sections or those of $^{206}_{82}$Pb and $^{207}_{82}$Pb can be related to known nuclear decays in the recoils. Also deduced was the number of K-shell vacancies per reaction as a function of atomic number, which varies from 0.1 to 1.7, with pronounced minima at the shell closures $Z = 50$ and 82. The system $^{181}_{73}\text{Ta} + \alpha$ at 18.5- and 20.5-MeV bombarding energy is studied in an x-ray-γ coincidence experiment selecting the $(\alpha,2n)$ reaction channel. A general procedure for complete cascade analysis is formulated. It emerges that $(101 \pm 13)\%$ and $(105 \pm 8)\%$ of the satellite intensity at 18.5 and 20.5 MeV, respectively, originate in converted transitions in the excited recoil. This accuracy shows that the study of converted continuum transitions by nuclear x-ray satellites is made possible by use of the algorithm for cascade analysis developed here. Also given are a decay scheme of $^{184}_{75}$Re, hitherto unknown, and a number of new transitions completing the decay scheme of $^{183}_{75}$Re.

I. INTRODUCTION

The majority of inner-shell ionization experiments are carried out at low projectile energies,[1] generally below the nuclear Coulomb barrier of the collision system under study. The possibility of nuclear excitation can therefore be ignored in the analysis of these experiments, except sometimes for Coulomb excitation of some low-lying states. Authors have occasionally corrected their ionization cross sections for the contribution from internal conversion after Coulomb excitation of the nucleus.[2-4] At higher bombarding energies, inelastic nuclear cross sections increase, and an analogous correction requires simultaneous recording of the nuclear γ rays along with the atomic deexcitation products such as x-rays or Auger electrons. Such a procedure then reveals the need of sometimes considerable corrections, e.g., 38% for K-shell cross sections of 9-MeV α particles on $^{169}_{69}$Tm (Ref. 3) and often corrections in the 10% range.

One should therefore be prepared to find nuclear contributions in the ionization of heavy elements if the projectile energies are above reaction threshold. Reactions involving a change of nuclear charge will thus lead to ionization of the residual atoms. If the relevant reaction cross section and the direct ionization cross section are comparable, additional x-ray lines should occur in the spectra. This situation prevails for the K-shell of heavy atoms. Indeed, K-x-ray spectra of heavy target elements found in the literature sometimes show such supplementary peaks.[5,6] Examples that will be studied in detail below are shown in Fig. 1. It was conjectured by some authors that one could assume internal conversion to be responsible for the phenomenon. Deconninck and Longequeue[7] and Deconninck *et al.*[8] drew attention to its widespread occurence at high projectile energies, and coined the term "nuclear satellites" for the additional x-ray lines.

Since then, various attempts have been made to assess quantitatively the observed intensity of the nuclear K-x-ray satellites.[9-12] We shall give in Sec. II extended information on our own attempts at this question. We reach the conclusion that we explain between 19% ($\alpha + ^{169}_{69}$Tm) and 92% ($\alpha + ^{181}_{73}$Ta) of the observed satellite intensity by internal conversion of known nuclear cascade transitions. The explained fraction often remains below 50%. The analysis of Berinde *et al.*[12] suffers from the partial lack of simultaneously recorded γ rays. Randell *et al.*[11] base their statements exclusively on the energy dependence of the satellite yield and do not attempt a more quantitative analysis. A rather detailed study is that of Deconninck and Longrée.[10] These authors work with the assumption that the average K-shell conversion coefficient $\bar{\alpha}_K$ of the residual nucleus in one reaction channel can be meaningfully carried over to the several other open channels. With this assumption they are able to explain the observed nuclear-satellite cross section. The essential uncertainty common to the studies reviewed thus far comes from the fact that more than one open reaction channel can contribute to the satellite yield. Therefore, residual nuclei are usually involved whose deexcitation cascade is insufficiently known.

This difficulty is avoided in the elegant experiment of Seyfarth *et al.*[13] on thermal neutron capture by $^{155}_{64}$Gd, $^{176}_{71}$Lu, and $^{199}_{80}$Hg. These authors

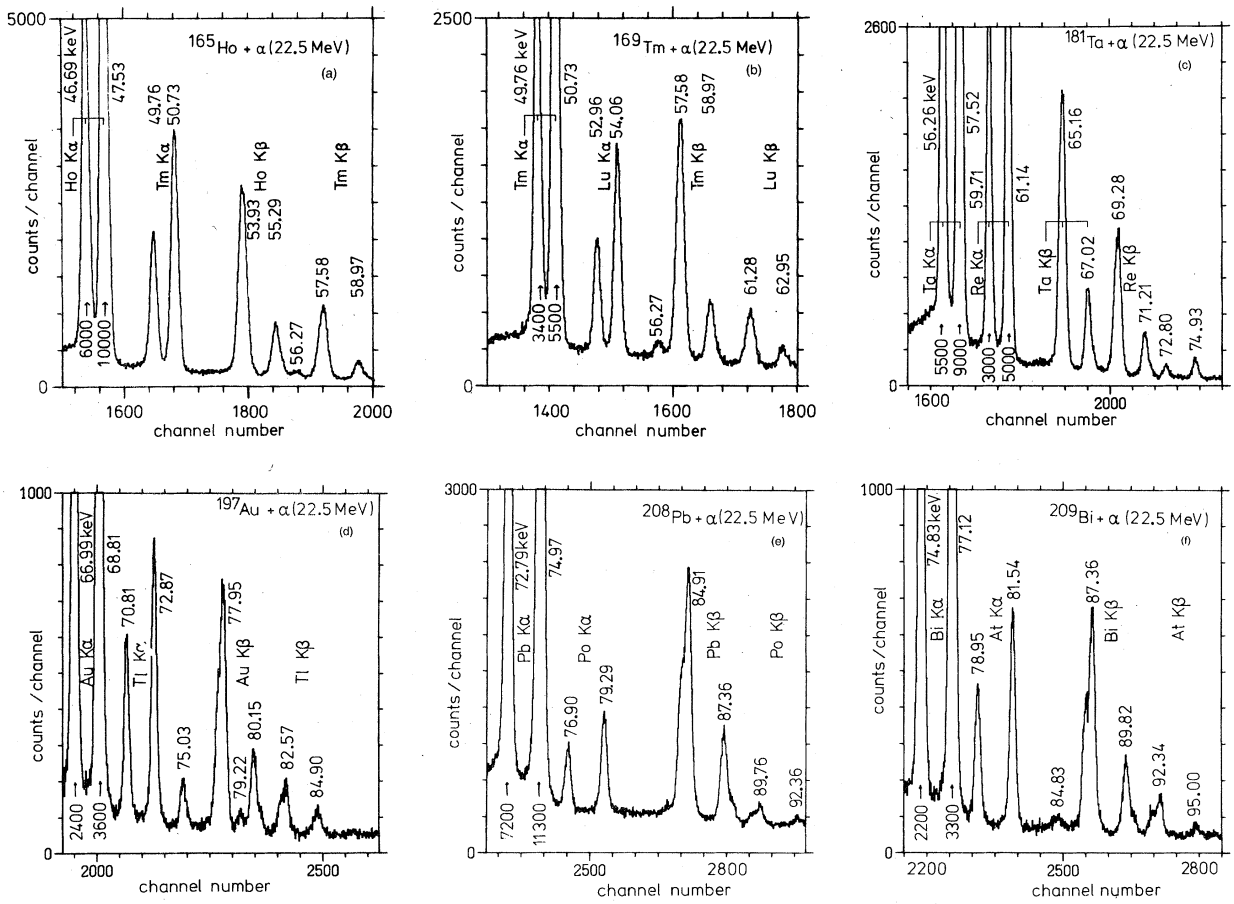

FIG. 1. K-x-ray singles spectra from 22.5-MeV α-particle bombardment of various targets. (a) $^{165}_{67}$Ho. The 56.27-keV line is Ta $K\alpha_2$. The target was mounted on a Ta frame. (b) $^{169}_{69}$Tm. The 56.27-keV line is again Ta $K\alpha_2$. (c) $^{181}_{73}$Ta. The 72.80-keV and 74.93-keV lines are attributed to Pb $K\alpha_2$ and $K\alpha_1$, respectively, originating in the Pb contained in the Al chamber walls. (d) $^{197}_{79}$Au. The 75.03-keV line is again attributed to Pb $K\alpha_1$. The 79.22-keV line is probably an unknown γ, and may also contain some Po $K\alpha_1$ produced by alpha particles in the Pb content of normal Al material. (e) $^{208}_{82}$Pb. (f) $^{209}_{83}$Bi. The 84.83-keV line is again Pb $K\beta_1'$. The pair of lines $K\alpha_1$, $K\alpha_2$ is always labeled by $K\alpha$, the pair $K\beta_1'$, $K\beta_2'$, by $K\beta$. The energies assigned to the peaks are from our own peak fitting and calibration, and are uncertain by 0.03 keV.

find that 83–105% of the observed K-x-ray intensity are accounted for by conversion of discrete nuclear γ transitions.

The charged-particle experiments and the neutron-capture experiment, however, differ in the primary angular momentum population which is limited to lower values in the slow-neutron reaction. Increased conversion in the continuum region of the residual nuclei produced by charged particles as compared to the cases investigated by Seyfarth *et al.*[13] is therefore conceivable. In order to study the question without ambiguity we have designed the coincidence experiment and the method of analysis on which the present paper is centered and which are described in Secs. III and V below.

The cross sections of charged-particle-induced nuclear satellites deserve an adequate quantitative treatment for two supplementary reasons: (i) The study of the continuum region of nuclei by conversion electron spectroscopy has yielded first interesting results[14] on the multipole character of the deexcitation in $^{160}_{66}$Dy. But the transitions below 800 keV are excluded[14] from this analysis owing to instrumental cutoff. There would be an inherent advantage in using nuclear x-ray satellites to identify continuum conversion, since the contributions of all converted continuum transitions down to the K-shell binding energy are lumped together in just the K-x-ray satellite lines. This increases sensitivity and includes automatically the lowest transitions. (ii) Inner-shell vacancies set off Auger cascades in the electron shells that can lead to high-charge states of atoms recoiling into vacuum.[15-17] Nuclear K-x-ray satellite intensities provide a convenient mea-

sure of the rate of "ignition" of the cascades in the K shell. A quantitative understanding of the satellite cross sections will allow predictions on the charge states of recoiling atoms to be made.

Section II outlines our analysis of nuclear-satellite cross sections without the selection of a specific reaction channel. In Sec. III the technique of the coincidence experiment is described, with the data reduction in Sec. IV. The quantitative analysis of the coincidence data is developed in detail and results are given in Sec. V. Finally, the results are discussed and conclusions are drawn in Sec. VI.

II. NUCLEAR-SATELLITE INTENSITIES: SURVEY

A. General

It becomes evident from the example shown in Fig. 2 why it is difficult to derive conclusive information on the origin of the nuclear-satellite radiation from cross section measurements alone. The Coulomb barrier for α particles on heavy elements is usually located several MeV above the (α, n) reaction threshold, e.g., about 5.5 MeV in the case of $^{181}_{73}$Ta. Reactions therefore populate the residual nucleus at high excitation as soon as they effectively set in. Controlled population of a low-excitation region is possible only for the $(\alpha, 2n)$ channel. But a reliable correlation of satellite intensity with the γ cascade is then excluded since the deexcitation scheme of the residual nuclei of the (α, n) reaction is not well known in the relevant mass range.

The knowledge of empirical satellite cross sections is nevertheless quite useful in some applications, as explained in Sec. I. With the aim to establish systematics we have therefore explored the cross sections for a number of heavy targets bombarded by α particles: $^{120}_{50}$Sn, $^{165}_{67}$Ho, $^{169}_{69}$Tm, $^{181}_{73}$Ta, $^{197}_{79}$Au, $^{206}_{82}$Pb, $^{207}_{82}$Pb, $^{208}_{82}$Pb, and $^{209}_{83}$Bi. The nuclear γ rays were recorded concurrently.

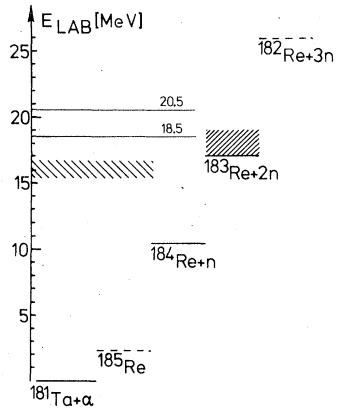

FIG. 2. Schematic energy diagram showing the accessible excitation regions in the case of $^{181}_{73}$Ta target as a function of α-particle energy. The hatched area around $E_{LAB} = 16$ MeV marks the effective Coulomb barrier, the hatched area in ^{183}Re is the spectroscopically known region.

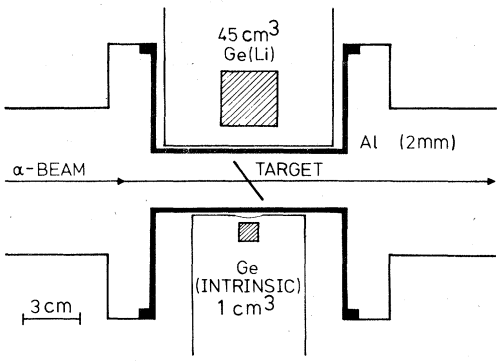

FIG. 3. Detector and target geometry, schematically. Distances are drawn approximately to scale.

B. Cross sections

The satellite and γ-ray production cross sections are measured in the geometry and with the detectors shown in Fig. 3. We postpone giving more technical details until we describe the coincidence experiment in Sec. III. In Table I are listed some of the experimental parameters: targets, target thicknesses, and beam energies. The resulting nuclear-satellite cross sections $\sigma_I(Z+2)$ are shown in Fig. 4, which also displays the relevant nuclear-reaction cross sections.[18-25] There is an additional cross section $\sigma_I(\text{Te}) = (90 \pm 30)$ mb, not shown in the figure, for $^{120}_{50}$Sn at 22.5 MeV. It is seen that the energy dependence of the satellite cross section is correlated with that of the summed reaction cross section. But there is no simple

TABLE I. Target information.

Target	Thickness (μg/cm^2)
$^{120}_{50}$Sn	39.9
$^{165}_{67}$Ho	130.9
$^{169}_{69}$Tm	71.2
$^{181}_{73}$Ta	2959.0
$^{197}_{79}$Au	191.0
$^{206}_{82}$Pb	309.0
^{207}Pb	607.0
^{208}Pb	625.0
$^{209}_{83}$Bi	260.0

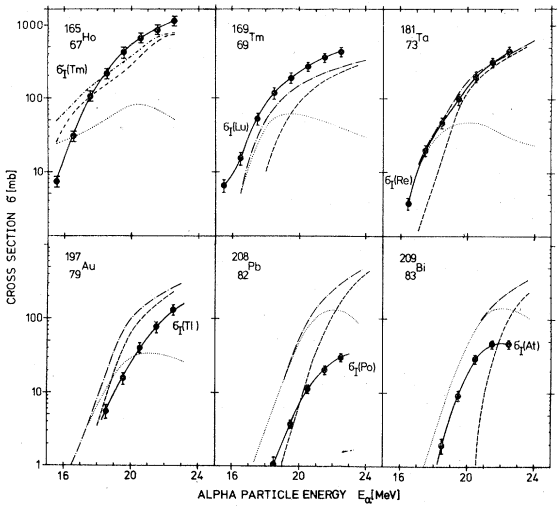

FIG. 4. Cross section σ_I of nuclear satellite K-shell vacancy production. The solid line is only drawn to connect the experimental points. Also plotted are the reaction cross sections (Refs. 18–25) for (α,n) (dotted line) and $(\alpha,2n)$ (dashed line), and their sum (dash-dotted line). The only data point obtained for $^{120}_{50}$Sn, σ_I(Te) = (90 ± 30) mb at 22.5 MeV, is not shown in this figure.

relation between the absolute magnitudes of the two.

The γ rays recorded concurrently with the x-rays are converted into production cross sections for the individual lines identified[26-33] as belonging to the deexcitation of the residual nucleus, mostly in the $(\alpha, 2n)$ channel. Appropriate angular distribution corrections are applied. We renounce to listing the individual γ-ray cross sections here. They enter the analysis presented in Sec. II C.

Before turning to this, we note in passing that nuclear satellites originate from an atom with unperturbed static K-shell fluorescence yield.[34] We find within the experimental errors ranging from 3 to 15% for the satellite radiation the same ratios of radiative-transition rates $K_{\alpha_2}/K_{\alpha_1}$, $K_{\beta_1'}/K_{\alpha_1}$, and $K_{\beta_2'}/K_{\alpha_1}$ as in fluorescence spectra.

Higher incident energies are required to obtain measureable intensities $\sigma_I(Z+1)$ besides $\sigma_I(Z+2)$ as they result from (α, pxn) reactions. For instance, both $_{83}$Bi and $_{84}$Po K x rays are observed[10] when $_{82}$Pb is bombarded by 60-MeV α particles, and $\sigma_I(Z+1)$ and $\sigma_I(Z+2)$ are of comparable magnitude at 110 MeV.

C. Correlation with γ-ray data and with reaction cross sections

For the targets we investigate (Table I), decay-scheme information[26-33] is available almost exclusively for the residual nucleus of the $(\alpha, 2n)$ reaction. We therefore have to be prepared that we might not be able to explain all of the observed satellite cross section $\sigma_I^{\exp}(Z+2)$ by K-shell internal conversion in the known cascade. We proceed as follows: For a given residual nucleus, each individual γ-ray cross section σ_j^i (for transition from level i to level j) is multiplied by the K-shell conversion coefficient $(\alpha_K)_j^i$ for this transition. Summation over all known transitions in the residual nucleus yields the expected nuclear-satellite cross section

$$\sigma_I^{\text{calc}}(Z+2) = \sum_{i,j} \sigma_j^i (\alpha_K)_j^i . \tag{1}$$

In performing this summation we have assumed that K-shell vacancies are filled between consecutive conversions in the cascade. The lifetime of the K-shell vacancy[34] varies from $\tau_K = 8\times10^{-17}$ to 1×10^{-17} sec between Sn and Bi, while electromagnetic lifetimes in heavy nuclei are of the order 10^{-12}–10^{-9} sec. The assumption is therefore well justified. It is also supported by the unperturbed radiative-transition rates found for the satellites (see Sec. II B). The ratio

$$r \equiv \sigma_I^{\text{calc}}(Z+2)/\sigma_I^{\exp}(Z+2) \tag{2}$$

is the fraction of satellite cross section explained by conversion in the known cascade. This quantity r is constructed in a sample calculation for the $^{181}_{73}$Ta target and 20.5-MeV incident energy in Table II. The intensities are based on the γ-ray spectrum, part of which is shown in Fig. 5. The higher-energy transitions, not shown in Fig. 5, are recorded in the 45-cm^3 detector. The resulting r is given in Table III for this and the other cases studied in the present work, along with information on the residual nucleus excitation region[26-33] covered by the recorded γ transitions. In the measurement on $^{181}_{73}$Ta, we discovered 11 γ transitions in $^{183}_{75}$Re not previously known.[28,35] They are included in the values of r in Table III. Their position in the decay scheme is given, after the description of the coincidence experiment, in Sec. V E. All information on the multipolarities of the γ transitions is taken from the references given in Table III. Where such information is not available the lowest multipole order compatible with spin-parity of the initial and final levels is adopted in evaluating Eq. (1). In the Ta measurement, we found 20 transitions in $^{184}_{75}$Re not known before.[29] Their position in the decay scheme is given in Sec. V E. We did not find it meaningful to include them in the value of r in Table III, as assumptions on the multipolarity of the transitions are too uncertain in this case. As can be seen from Table III and Eq. (2), we explain in general only part of the satellite intensity by conversion in a known cascade, in one case as little as 19%

TABLE II. Sample calculation of the ratio r according to Eq. (2), for $^{181}_{73}$Ta target at 20.5-MeV incident energy. The transitions are numbered by μ; σ_μ is the γ-ray cross section for transition μ. The new transitions found in our coincidence experiment are marked by an asterisk. Their multipolarity is taken to be the lowest one compatible with the spin-parity of the levels involved. Transitions are in ^{183}Re only (see text).

μ	Energy (keV)	Multipolarity	$\alpha_K^{(\mu)}$ [a]	$B_\mu \equiv \frac{\sigma_\mu \times 10^2}{\sigma_I^{\exp}(Z+2)}$	$\alpha_K^{(\mu)} B_\mu$
*1	102.2	$E2$	0.862	0.331	0.29
2	114.7	$M1+(2.2\%)E2$	2.990	16.33	47.85
*3	128.5	$M1$	2.152	0.206	0.44
4	141.4	$E2$	0.416	4.29	1.79
5	145.4	$M1+(2.2\%)E2$	1.492	8.92	13.31
6	167.7	$M1+(3.7\%)E2$	0.987	7.48	7.38
7	175.3	$M1+(1.6\%)E2$	0.885	7.72	6.83
*8	181.9	$E1$	0.0682	1.71	0.12
9	196.9	$M1+(3.7\%)E2$	0.630	4.61	2.90
10	203.5	$M1+(1.8\%)E2$	0.583	4.00	2.33
11	223.4	$M1+(3.9\%)E2$	0.443	2.17	0.96
*12	230.0	$M1$	0.439	0.462	0.20
13	231.3	$M1+(1.6\%)E2$	0.410	2.06	0.84
14	250.1	$M1+(2.0\%)E2$	0.329	1.07	0.35
15	256.4	$M1+(1.0\%)E2$	0.310	1.06	0.33
16	258.8	$E2$	0.0862	1.41	0.12
17	263.7	$E2$	0.0820	3.01	0.25
18	273.3	$M1+(4.0\%)E2$	0.255	0.467	0.12
*19	276.9	$M1$	0.253	0.875	0.22
20	282.2	$M1+(1.4\%)E2$	0.238	0.771	0.18
*21	295.2	$M1$	0.213	0.979	0.21
22	304.2	$M1+(3.2\%)E2$	0.192	0.247	0.05
*23	306.8 [b]			0.548	
24	321.0	$E2$	0.0491	2.18	0.11
25	325.8	$M1+(0.8\%)E2$	0.162	0.214	0.03
26	365.2	$E2$	0.0354	0.959	0.03
27	378.5	$E2$	0.0324	2.15	0.07
28	380.0	$E2$	0.0321	0.917	0.03
29	381.9	$E1$	0.0113	22.27	0.25
30	420.4	$E2$	0.0251	0.685	0.02
31	435.5	$E2$	0.0230	1.66	0.04
*32	448.6 [b]			1.36	
33	474.3	$E2$	0.0188	0.271	0.01
34	484.7	$E1$	0.0066	17.16	0.11
35	488.0	$E2$	0.0176	0.776	0.01
36	489.0	$E2$	0.0175	0.259	0.00
*37	503.2 [c]	...	...	0.0	0.0
38	524.1	$E2$	0.0150	0.380	0.01
39	539.0	$E2$	0.0140	0.832	0.01
40	585.6	$E2$	0.0117	0.853	0.01
*41	589.0 [c]	...	...	0.0	0.0
42	630.4	$E2$	0.0100	0.250	0.00
43	678.8	$E2$	0.0085	0.574	0.00
44	737.0	$M1$	0.0194	0.288	0.01
45	851.0	$M1$	0.0135	1.96	0.03

$r = 10^{-2} \sum_\mu \alpha_K^{(\mu)} B_\mu = 0.8785$

[a] Values taken from Ref. 37.

[b] Multipolarities not assigned, owing to lack of spin-parity information.

[c] Transition known only from the coincidence data. The B_μ is therefore set equal to zero.

($^{169}_{69}$Tm). We observe, however, that r generally increases with bombarding energy. This suggests that the lack of information about the (α, n) channel is mainly responsible for the deviation of r from unity.

A very useful way to view the satellite data is to correlate them with the reaction cross section. This is displayed in Fig. 6 where the satellite

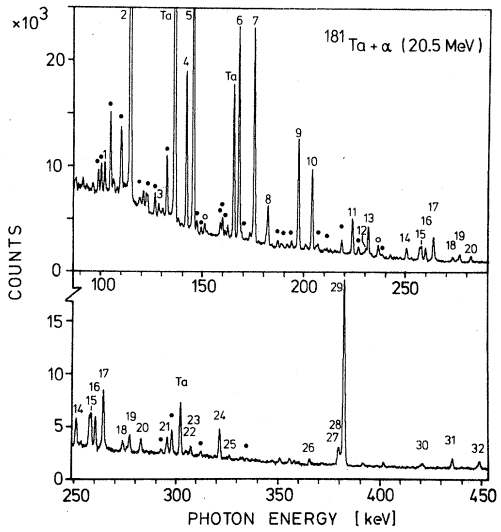

FIG. 5. γ-ray spectrum of $^{181}_{73}$Ta + α at 20.5 MeV, up to 450 keV, taken by the 1-cm^3 intrinsic Ge detector. The numbering of the peaks corresponds to that of Table II. Peaks labeled by an open circle are transitions in ^{183}Re whose position in the decay scheme could not be determined. They give a negligible contribution to the internal conversion sum of Table II. Full dots mark transitions in ^{184}Re, including five whose position in the decay scheme could not be determined. The Ta lines are from target Coulomb excitation.

cross sections, at 1 MeV above the $(\alpha, 2n)$ threshold divided by $(\sigma_{\alpha,n} + \sigma_{\alpha,2n})$, are plotted against atomic number. This cross section ratio is just the number of K-shell vacancies in the recoil created per reaction event, or average K-x-ray multiplicity. The nuclear cross sections used in this plot are taken from Refs. 18–25. There is an additional data point of 0.12 K-shell vacancy per reaction (not plotted in Fig. 6) for the target $^{120}_{50}$Sn at 8 MeV above the $(\alpha, 2n)$ threshold. This is the lowest energy at which we observe a nuclear-satellite peak for Sn. The data points show a roughly exponential dependence on atomic number for $Z = 69$ to 82. Taken together with the data point for Sn, they show two clear minima of 0.1 K vacancy per reaction at $Z = 50$ and 82, and there is a maximum of 1.7 K vacancies per reaction at $Z = 69$.

III. EXPERIMENTAL TECHNIQUE

A. Geometry and detectors

The target and detector arrangement shown in Fig. 3 is used in both the singles measurements reported on in Sec. II B and in the coincidence experiment which will now be described. A 45-cm^3 Ge(Li) detector, for γ-ray counting, and a 1-cm^3 intrinsic Ge detector, for x-ray and low-energy γ-ray counting, are viewing the target under 90° from 17-mm distance through the 2-mm Al window of the target chamber. The 18.5–20.5-MeV ^{4}He beam of 5–15 nA, provided by the HVEC-FN tandem of the University of Köln, is focused onto the Ta-foil target, which is inclined 45° with respect to the beam. The beam is stopped 3 m downstream in an insulated Faraday cup.

The intrinsic Ge detector has 550-eV energy resolution at Ta $K\alpha$ of 57 keV, and at 6 kHz and 1.5-μsec shaping time constant in the main amplifier. Knowledge of the absolute detection efficiency of both the 45-cm^3 and the 1-cm^3 detectors is important. It is measured by placing radioactive point sources in target position. Sources of ^{57}Co, ^{133}Ba, ^{152}Eu, and ^{241}Am with calibrated activity (purchased from the Radiochemical Centre Ltd., Amersham, U.K.; and Physikalisch-Technische Bundesanstalt, Braunschweig, Germany) are used to measure the efficiency up to 444 keV for the intrinsic Ge detector, and up to 779 keV for the Ge(Li) detector. Graphic interpolation permits to read the efficiency for any energy in this range with an estimated accuracy of 5%. The values of detector solid angle, absorption in the Al windows, and detector housing are incorporated in the experimental efficiency points shown in Fig. 7.

B. Coincidence electronics

Coincident x-ray–γ events are selected by a standard fast-slow circuit with constant fraction timing. The experiment determines absolute intensities of both coincidence and singles events. This requires that special attention be given to dead-time measurement and coincidence efficiency.

The 1-cm^3 intrinsic Ge diode is coupled to a pulse-optical-feedback preamplifier. The "inhibit" signal is used as a gate to interrupt data acquisition for the duration of preamplifier reset. Total dead time is measured by feeding coincident pulser signals at a beam-current-controlled rate into the test input of the preamplifiers. From the number of pulser signals surviving in the spectra, both singles and coincidence dead time are deduced. They are, e.g., in the 20.5-MeV run at 6- and 7-kHz singles rates, 19% in the Ge(Li) branch, 13% in the branch of the small intrinsic Ge diode, and 10% for the coincidences. Coincidence dead time is smaller owing to the priority of coincidence events in the computer.

Time resolution, when optimized for 500-keV γ rays in the Ge(Li), is 18 nsec (FWHM). It is 2.8 nsec for the pulser signals. γ transitions down to 100 keV are important in our analysis.

TABLE III. Summary of the analysis of satellite intensities in the cross section measurements of x-rays and nuclear γ rays. The γ-ray intensities are corrected for the angular distribution. The ratio r is defined in Eq. (2). We call n the number of γ transitions considered in the analysis, and ϵ the excitation region known from spectroscopy. The maximum excitation allowed by kinematics is ϵ_{max}.

		$(\alpha, 2n)$ residual nucleus			(α, n) residual nucleus			
Target	E_α (MeV)	ϵ_{max} (MeV)	ϵ (MeV) (n)	Ref.	ϵ_{max} (MeV)	ϵ (MeV) (n)	Ref.	r [a]
$^{120}_{50}$Sn			^{122}Te			^{123}Te		
	22.5	7.26	2.80 (none)	29	14.19	0.25 (none)	29	...
$^{165}_{67}$Ho			^{167}Tm			^{168}Tm		
	17.5	0.99	1.86 (48)	26	7.81	0 (none)	...	0.25
	18.5							0.58
	19.5							0.62
	20.5							0.68
	21.5							0.74
	22.5	5.84			12.71			0.66
$^{169}_{69}$Tm			^{171}Lu			^{172}Lu		
	18.5	0.99	2.02 (108)	27	7.91	0 (none)	29	0.19
	19.5							0.26
	20.5							0.49
	21.5							0.61
	22.5	4.90			11.82			0.78
$^{181}_{73}$Ta			^{183}Re			^{184}Re		
	18.5	1.73	2.39 (45)	28 and this work	8.09	0.91 (none)	29 and this work	0.33
	19.0							0.49
	19.5							0.63
	20.5							0.88
	22.5	5.65			12.01			0.92
$^{197}_{79}$Au			^{199}Tl			^{200}Tl		
	22.5	5.32	2.08 (28)	29	12.30	0.75 (2)	29	0.47
$^{206}_{82}$Pb			^{208}Po			^{209}Po		
	22.5	2.04	2.70 (3)	30	9.01	4.27 (14)	31	0.27
$^{207}_{82}$Pb			^{209}Po			^{210}Po		
	18.5	...	4.27 (7)	31	6.00	5.06 (22)	32	0.37
	19.5	...						0.38
	20.5							0.38
	21.5							0.44
	22.5	2.27			9.92			0.52
$^{208}_{82}$Pb			^{210}Po			^{211}Po		
	22.5	2.55	5.06 (10)	32	7.11	1.43 (7)	29	0.28
$^{209}_{83}$Bi			^{211}At			^{212}At		
	18.5	...	2.48 (none)	29, 33	2.87	0.23 (none)	29	...
	19.5	...						
	20.5	...						
	21.5							
	22.5	1.73			6.79			...

[a] The errors are estimated to be about 20%.

We must therefore admit into the timing electronics the whole range of different rise times due mainly to the low-energy photons in the Ge(Li). This leads to a shift of the prompt peak in the time spectrum with varying photon energy. The reason of this shift is that for the slowest pulses the time signal in the constant-fraction timing discriminator (CFTD) can only be generated at the leading edge of the pulse, and therefore shifts with photon energy. The result is the broad distribution of true coincidences in the time spectrum of Fig. 8 which disappears completely when operating the CFTD in the "slow-rise-time-reject" mode. For the absolute measurement of coincidence inten-

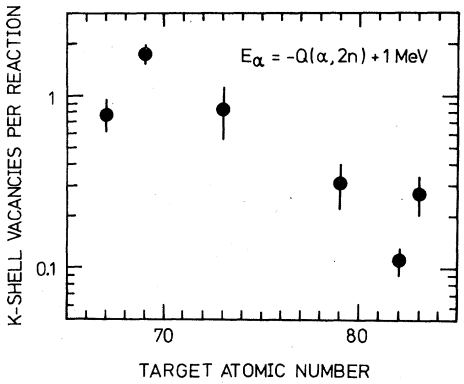

FIG. 6. Number of K-shell vacancies per reaction event vs atomic number, taken 1 MeV above the $(\alpha, 2n)$ threshold. The minimum at the shell closure $Z = 82$ is clearly visible. The data point for $^{120}_{50}$Sn is not plotted, since it could be measured only 8 MeV above the threshold. The value is 0.12 vacancy per reaction, which marks another minimum at the $Z = 50$ shell closure.

sities, however, this elimination of true events is not permissible. It would introduce an unknown coincidence efficiency into the measurement. At the true-to-random ratio of 10 : 1 (at 20.5 MeV) and 6 : 1 (at 18.5 MeV) the broad distribution of true events presents no difficulty in data reduction. We make sure that coincidence efficiency is unity down to threshold by gating a γ reference line by the CFTD output and comparing gated to ungated intensity. Data are recorded in event-by-event mode on magnetic tape by a PDP-11 computer.

IV. DATA REDUCTION

Intensities of x- and γ-ray lines needed to evaluate Eq. (2) are obtained from a peak-fitting routine treating the lines as Gaussian shaped with exponential tails, and fitting a third-order polynomial plus step functions at the peak positions to the background. The individual line intensities are corrected for detection efficiency. In the x-ray spectra, the intensity is then summed over $K\alpha_{1,2}$ and $K\beta'_{1,2}$ lines.

The x-ray–γ coincidences in the Ta experiment are selected in several steps. After subtraction of random background an energy window in the x-ray spectrum is set on the K lines of $_{73}$Ta and $_{75}$Re. As this spectrum contains a continuous background, mainly from Compton scattering of high-energy photons in the 1-cm^3 Ge detector, an equivalent energy window adjacent to the K-x-ray region is set. Subtraction of the two γ spectra corresponding to the two window settings in the x-ray spectrum yields a γ-ray spectrum containing the coincidence intensities needed in the analysis.

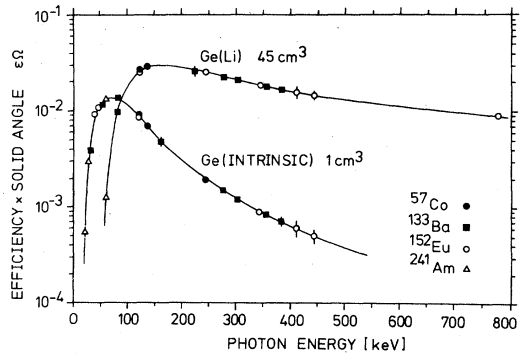

FIG. 7. Photopeak efficiency of both the 1-cm^3 intrinsic Ge and the 45-cm^3 Ge(Li) detectors, measured with calibrated sources in target position.

Replacing the window on the K x rays by windows on the well resolved low-energy γ lines also recorded in the 1-cm^3 intrinsic Ge detector reveals a large number of previously unknown[28,35] γ-γ coincidences. They are summarized in Sec. V E below.

V. QUANTITATIVE CASCADE ANALYSIS FROM COINCIDENCE DATA

A. General

The nuclear K–x-ray satellite quanta carry no signature characteristic of the particular nuclear

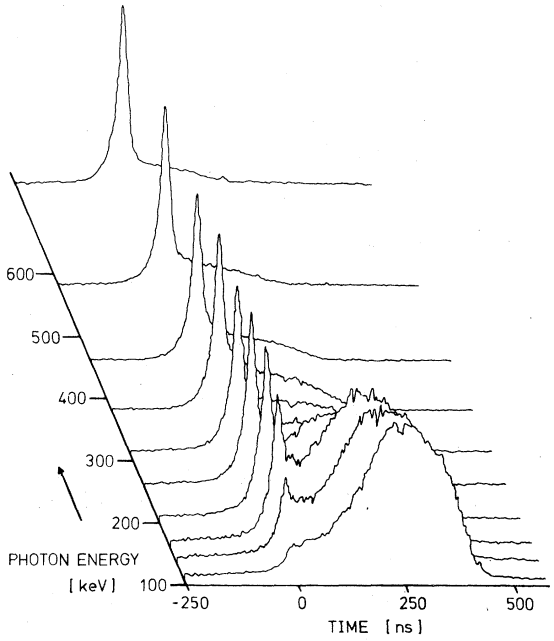

FIG. 8. Time spectra of coincidences of Ta and Re K x rays with γ rays. The energy axis refers to photons recorded in the Ge (Li). Time resolution, 18 nsec, is optimized for 500 keV, and is 2.8 nsec for pulser signals.

transition in which the relevant K-shell vacancy is created. Only the condition of simultaneity of the x and γ rays permits measured satellite intensity to be attributed to a specific cascade path. Identification with a particular transition is, however, not possible. A certain "bookkeeping" scheme has therefore to be set up. The aim is to use the measured population of the selected residual nucleus and the known deexcitation scheme to calculate K-x-ray production by internal conversion. The result is then compared to the experimental nuclear-satellite intensity filtered out by requiring coincidence with transitions in the selected residual nucleus. We choose the transitions in the $(\alpha, 2n)$ reaction product for this purpose.

B. Ground-state transitions

To introduce notation which can easily be used in a generalized analysis (see Appendix) we express, first, the measured intensity of coincidences, ${}^cI_j^i$, between a chosen γ ray from level i to level j and a nuclear-satellite x ray as

$$ {}^cI_j^i = S_j^i {}^sI_j^i . \tag{3}$$

Here ${}^sI_j^i$ (with $i<j$) is the simultaneously emitted γ-singles intensity of the selected transition $i \rightarrow j$. It is connected to the actually recorded number ${}^sN_j^i$ of quanta γ_j^i in the detector at angle θ_γ and of efficiency $(\epsilon\Omega)_j^i$ at energy E_j^i by

$$ {}^sN_j^i = {}^sI_j^i W_j^i(\theta_\gamma)(\epsilon\Omega)_j^i T_\gamma ,$$

where $W_j^i(\theta_\gamma)$ is the angular distribution of γ_j^i. In an analogous fashion and with evident notation we have

$$ {}^cN_j^i(\theta_\gamma, \theta_x) = {}^cI_j^i W_j^i(\theta_\gamma) W_x(\theta_x)(\epsilon\Omega)_x(\epsilon\Omega)_j^i T_c .$$

The factors T_c and T_γ are dead-time corrections for the coincidence and singles rates, respectively. Since dead time is assumed to be independent of E_j^i, we apply a unique γ-singles dead-time correction for all γ_j^i.

The quantity S_j^i is thus the *sum* of probabilities along the cascade path for satellite x-ray emission coincident with γ transition $i \rightarrow j$ forming part of this cascade path. The coincidence experiment yields, according to Eq. (3), a value of $S_j^i(\text{exp})$ for every γ_j^i transition for which the coincident x-ray intensity can be determined:

$$ S_j^i(\text{exp}) = {}^cI_j^i / {}^sI_j^i = {}^cN_j^i T_\gamma / {}^sN_j^i \, T_c(\epsilon\Omega)_x . \tag{4}$$

We have used $W_x(\theta_x)=1$ to express that we treat the K-x-ray emission as isotropic.[36] The $S_j^i(\text{exp})$ is thus, according to Eq. (4), immediately accessible from experimental data. We then construct the calculated counterpart of $S_j^i(\text{exp})$, which we shall call $S_j^i(\text{calc})$, from the measured γ-singles intensities and the theoretical internal conversion coefficients. Owing to the complexity of the decay scheme this is a somewhat complicated task for an arbitrary choice of γ_j^i. The general case will therefore be developed in the Appendix.

We demonstrate the principle in the special case that γ_j^i is chosen to be γ_0^i, a ground-state transition. It is understood that the levels are numbered in order of increasing energy, starting with $j=0$ for the ground state. The general case is a straightforward, though complex, extension of the procedure developed for γ_0^i and where the accuracy lost in the restriction to the ground-state transition is recovered.

Let the residual nucleus have only one ground-state transition γ_0^1. In this case, the summed x-ray emission probability is given by

$$ S_0^1(\text{calc}) = \frac{{}^cI_0^1(\text{calc})}{{}^sI_0^1} = \sum_{\substack{i,j \\ j\neq 0}} \frac{\omega_K (\alpha_K)_j^i \, {}^sI_j^i}{[1+(\alpha_{\text{tot}})_0^1]\,{}^sI_0^1} \equiv \sum_{\substack{i,j \\ j\neq 0}} \frac{\omega_K (\alpha_K)_j^i \, {}^sI_j^i}{A_0^1} , \tag{5}$$

where $(\alpha_K)_j^i$ is the K-shell conversion coefficient of transition γ_j^i and $(\alpha_{\text{tot}})_0^1$ the total conversion coefficient of the selected ground-state transition γ_0^1. The factor $1+(\alpha_{\text{tot}})_0^1$ appears in the denominator of Eq. (5) because only the fraction $1/[1+(\alpha_{\text{tot}})_0^1]$ of the x rays coincident with transition γ_j^i involve a γ ray (and not a conversion electron) for the ground-state transition. The ω_K is the K-shell fluorescence yield of the residual atom, of atomic number $Z+2$ in the present experiment. The summation in Eq. (5) extends over all known transitions γ_j^i coincident with an x-ray satellite except the ground-state transition γ_0^1. We have introduced the abbreviation

$$ A_j^i \equiv {}^sI_j^i[1+(\alpha_{\text{tot}})_j^i] \tag{6}$$

for total intensity of transition $i \rightarrow j$. If levels i and j are not connected by a transition, we have, of course, $I_j^i=0$, $A_j^i=0$.

In our actual experiment on Ta, the residual nucleus ^{183}Re has several ground-state transitions[28]: 114.7, 258.8, and 851.0 keV. The direct comparison of $S_0^i(\text{exp})$ and $S_0^i(\text{calc})$ is not immediately possible since $S_j^i(\text{calc})$ can, in general, not be obtained by a direct generalization of Eq. (5) (see Appendix). The S_0^i occur, however, in the following sum of satellite x-ray intensity:

$$ \xi_K^{\text{calc}} \equiv \sum_{i=1}^{N} S_0^i(\text{calc}) A_0^i = \sum_{\substack{i,j \\ j\neq 0}} \omega_K (\alpha_K)_j^i \, {}^sI_j^i , \tag{7}$$

where N is the number of the highest level with a known γ decay in the cascade. In general, the

sum over i contains only a few nonvanishing terms since most $A_0^i = 0$, according to the definition (6). Equation (7) is readily obtained by taking S_0^i(calc) to be the calculated counterpart of S_0^i(exp) from Eq. (4) and by noting that both the first and the second part of Eq. (7) just express the total x-ray intensity ξ_K in cascade paths containing ground-state transitions. There is no term-by-term correspondence in the sums of Eq. (7). We will rederive Eq. (7) from the general scheme of cascade analysis in the Appendix.

The comparison with experiment is now carried out via the x-ray yield ξ_K instead of the individual probability sums S_0^i. We have

$$\xi_K^{\exp} \equiv \sum_{i=1}^{N} S_0^i(\exp) A_0^i = \sum_{i=1}^{N} \left(\frac{{}^cN_0^i}{T_c(\epsilon\Omega)_x} \frac{1+(\alpha_{\rm tot})_0^i}{W_0^i(\theta_\gamma)(\epsilon\Omega)_0^i} \right), \quad (8)$$

where S_0^i has been expressed according to Eq. (4).

The ratio

$$R_0 \equiv \xi_K^{\rm calc} / \xi_K^{\exp} \quad (9a)$$

is the fraction of observed nuclear K-x-ray satellite yield explained by internal conversion in the known discrete cascade. We have evaluated R_0 of Eq. (9a) at $E_\alpha = 18.5$ and 20.5 MeV using the experimental quantities ${}^sN_j^i$, ${}^cN_j^i$, T_γ, T_c, $(\epsilon\Omega)_j^i$, and $(\epsilon\Omega)_x$ derived from our Ta measurement in the way described in Sec. IV. There are some additional quantities need to evaluate R_0: The K-shell fluorescence yield of $_{75}$Re is taken[34] to be $\omega_K = 0.959$. The γ-ray angular distribution parameters A_2 and A_4 for the transitions in ^{183}Re are taken from the work of Singh *et al.*[28] who studied the ^{181}Ta$(\alpha, 2n\gamma)^{183}$Re reaction at 27 MeV. The possible difference in the alignment of the states lower in the cascade is of minor importance since, with few exceptions, the anisotropies are small[28] and are partly averaged over in our close-detector geometry. The K-shell and total conversion coefficients α_K and $\alpha_{\rm tot}$ are taken from Hager and Seltzer[37] once the multipole character of the transitions is established.

We follow Singh *et al.*[28] in the assignment of multipolarities to the γ transitions in ^{183}Re. In several transitions of the (402) and the (514) bands[28] of ^{183}Re, Newton[35] had previously found some $E2/M1$ mixing. We have therefore recalculated the mixing parameter $\delta^2(E2/M1)$ from the experimental branching ratios of the levels in these bands. We take the crossover transitions to be pure $E2$ with the rotational value of the reduced transition probability. The mixing parameter $\delta^2(E2/M1)$ for the band with total angular momentum projection K is then

$$\frac{\delta^2}{1+\delta^2} = \left(\frac{E(\text{cascade})}{E(\text{crossover})} \right)^5 \frac{b}{A(I_i, K)},$$

where

$$A(I_i, K) = \langle I_i K 2\,0 | I_i - 2\,K \rangle^2 / \langle I_i K 2\,0 | I_i - 1\,K \rangle^2 .$$

E(cascade) denotes the energy of the transition from level with spin I_i to its next neighbor, and b is the experimental branching ratio T(crossover)/T(cascade). The conversion coefficients α_K or $\alpha_{\rm tot}$ of the mixed transitions are

$$(\alpha)_j^i = [\delta^2 \alpha(E2) + \alpha(M1)]/(1+\delta^2) .$$

For the lowest transitions in the (402) and (514) bands, δ^2 from the transition immediately above is employed.

This completes the list of quantities required to evaluate R_0 according to Eq. (9a). The numerical result is

$$R_0 = \begin{cases} 1.21 \pm 0.30, & E_\alpha = 18.5 \text{ MeV} \\ 0.91 \pm 0.16, & E_\alpha = 20.5 \text{ MeV} . \end{cases} \quad (9b)$$

We will discuss the origin of the error limits below, when giving the results of the generalized analysis.

C. Analysis of complete cascade

Internal K-shell conversion throughout the cascade can be followed more completely by introducing population probabilities P_{nm} and probabilities for x-ray production, $X(i\rightarrow)$ and $X(\rightarrow f)$. The necessary formalism developed in the Appendix permits to calculate the summed probabilities S_j^i(calc) individually and for an arbitrarily chosen transition γ_j^i by Eqs. (A4) and (A5). An appropriate average over all the ratios

$$R_j^i \equiv S_j^i(\text{calc}) / S_j^i(\exp) \quad (10)$$

can then be taken, which should result in a reduction of the error limits as compared to R_0 of Eqs. (9a) and (9b). The choice of the weighting factors in this average is to some extent arbitrary, but turns out, in the present set of data, to be quite uncritical. We have chosen ${}^cN_j^i / S_j^i(\exp)$ to be the weight of R_j^i in order to emphasize cascade paths with (i) abundant x-ray production (${}^cN_j^i$) and with (ii) small probability $S_j^i(\exp)$ for producing these x rays in the discrete part of the cascade. The latter aspect is meant to favor the identification of converted continuum transitions. Our choice of the weighting corresponds, after Eqs. (4) and (10), to the averaging

$$\bar{R} \equiv \left(\sum_{i,j} {}^sN_j^i \frac{S_j^i(\text{calc})}{S_j^i(\exp)} \right) \Big/ \sum_{i,j} {}^sN_j^i . \quad (11a)$$

The evaluation of the S_j^i after Eqs. (4) and (A4) requires the same quantities as already used for R_0. It is therefore sufficient to refer for their

origin to the description in Sec. IIB. It can be read as being valid for all (i,j) appearing in the actual cascade in ^{183}Re. The numerical results are

$$\bar{R}=\begin{cases}1.01\pm0.13, & E_\alpha=18.5\ \text{MeV}\\ 1.05\pm0.08, & E_\alpha=20.5\ \text{MeV}.\end{cases} \tag{11b}$$

The reduction of the error of $\bar{R}$ as compared to R_0 is due to the averaging of the individual ratios R_j^i in $\bar{R}$ of Eq. (11a), while the errors of the individual R_j^i are in some cases larger than for R_0.

D. Error limits

The following uncertainties are expressed by the error limits in Eq. (11b): (i) Peak areas in the x- and γ-ray spectra carry the statistical error and the uncertainty of background subtraction. This latter uncertainty is largest in the number of coincidence counts ${}^cN_j^i$ due to random background and Compton background. It is typically 20% at $E_\alpha=18.5$ MeV, and 10% at 20.5 MeV. (ii) We assign an uncertainty of 5% to both the x- and γ-ray efficiencies. (iii) Dead-time correction factors are uncertain, owing to background subtraction around the pulser peak in the spectra, by 3–5% at 20.5 MeV, and by 4–7.5% at 18.5 MeV. (iv) We have assigned a 2% uncertainty to the fluorescence yield[34] of $_{75}$Re, and zero uncertainty to the internal conversion coefficients of Hager and Seltzer.[37] (v) The γ-ray angular distributions $W_j^i(\theta_\gamma)$ are uncertain by 2–8%, with an exceptional 16% for the 365.2-keV transition, when calculated from the A_2 and A_4 of Singh *et al.*[28] (vi) Self-absorption of the x rays in the target is negligible, and K-shell ionization of the $_{75}$Re atoms recoiling in Ta can equally be neglected.

The errors ΔR_0 and $\Delta\bar{R}$ in Eqs. (9b) and (11b) are calculated from the constituent uncertainties just enumerated by error propagation. A modification is adopted for the intermediate step where the errors of the P_{nm} of Eq. (A5) are evaluated. Following up the error propagation through the recursion relations (A5) turns out to be too cumbersome. We vary instead A_n^{n+k} in Eq. (A5) within the error limits previously determined by error propagation, and obtain the distribution of the resulting values P_{nm}. The error ΔP_{nm} is read from the width of this distribution and further used to calculate ΔR by error propagation.

E. New nuclear transitions

As already mentioned at the end of Sec. IV, we were able to identify a number of weak low-energy transitions previously unknown. In Fig. 9(a) are shown the 11 new transitions in ^{183}Re fitted into the relevant part of the decay scheme of Ref. 28.

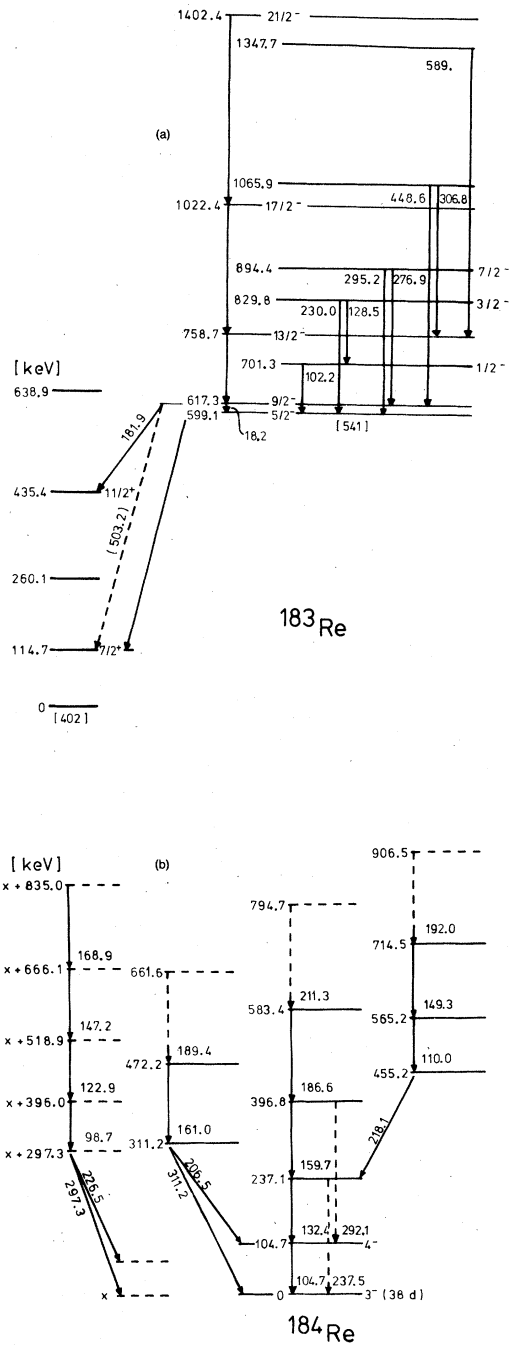

FIG. 9. (a) Partial decay scheme of ^{183}Re augmented by the new transitions found in the present coincidence experiment. The dashed transition is weak. The transitions not labeled by their energy are from Refs. 28 and 39. Spins of 701.3-keV, 829.8-keV, and 894.4-keV levels are those assigned by Lu and Alford (Ref. 38). (b) Tentative decay scheme of ^{184}Re constructed from the present coincidence measurement. Dashed transitions are weak. The symbol X represents an unknown excitation energy.

Spins are those of Refs. 28, 29, 38, and 39. The 18.2-keV distance between the 599.1- and 617.3-keV levels is derived from the 181.9-keV transition to the 435.4-keV $11/2^+$ level, and is confirmed by the pair transitions 295.2 and 276.9 keV from the $7/2^-$ level. This agrees within 1.2 keV with the level separation given by Lu and Alford.[38] Instead of the energy of 603 keV for the $5/2^-$ level given by these authors, Singh *et al.*[28] obtain 599.1 keV. Our measurement confirms this value within 0.3 keV. Figure 9(b) shows 20 new transitions in ^{184}Re arranged into a tentative decay scheme. Only the 104.7- and 83.4-keV transitions were previously known.[29] They served to identify the (α, n) channel in the coincidence experiment.

VI. DISCUSSION AND CONCLUSIONS

The combination of x- and γ-ray cross section measurements has yielded qualitative insight into the production mechanism of the nuclear K-x-ray satellites. It was possible to correlate energy and atomic-number dependence of the satellite yield with internal conversion in the residual nucleus of the (α, n) and $(\alpha, 2n)$ reaction channels. We found that the nuclear K–x-ray satellite cross section induced by α particles near the $(\alpha, 2n)$ threshold on heavy elements is generally of the order of the reaction cross section. The corresponding number of K-shell vacancies, i.e., the average K–x-ray multiplicity, exhibits a pronounced shell effect: from 0.1 vacancy per reaction at the shell closures $Z = 50$ and 82 it rises to a maximum of 1.7 per reaction in the deformed region around $Z = 70$. A correlation with the average level density in the recoil nucleus is evident. Between $Z = 69$ and 82 the effect of level density even overrides the increase of conversion coefficients with atomic number.

A similar behavior is observed[40] in the proton-induced nuclear K-satellite yield in the same mass range. There is, however, a much weaker atomic-number dependence: the number of K-shell vacancies per proton-induced reaction varies only[40] from 0.08 to 0.58, yet with maxima and minima at the same atomic numbers as in the present α particle data. We believe that the population of higher-angular-momentum states in the α-induced reactions causes this difference. It is therefore justified to presume that the average K–x-ray multiplicity will increase for heavier projectiles. This may well be of practical importance as one is thus able to control the rate of "ignition" of atomic Auger cascades in recoiling atoms.

From the considerable variation with Z of the number of K-shell vacancies per reation (Fig. 6), we see that some caution is advisable when operating with the concept of an *average* number of such vacancies[10] in several adjacent reaction channels. This may be justified only at incident energies where one channel dominates the reaction cross section. Similarly, we can see from Table III that also the concept of an *average* K-shell conversion coefficient[10] in neighboring nuclei demands some caution. When approaching with E_α the maximum of $\sigma_{\alpha,2n}$, one explains a higher fraction of the satellite yield by conversion of the known γ transitions. Yet, it is not the same fraction for different isotopes of the same target element.

A clearcut quantitative picture of the origin of the nuclear K-shell satellites emerges, however, only from the coincidence study presented in Secs. III–V of this paper. To our knowledge, the present work is the only such quantitative study carried out to date. (See, however, the note added in proof.) It shows [see Eq. (11b)] that within 8%, the observed nuclear K-shell satellite yield is due to internal conversion. This was expected from the qualitative trends observed in the various cross section measurements (Table III and Refs. 7–11, 40). At the same time, this result proves that, at the low bombarding energies of the present experiment, where the continuum region is practically not populated, we dispose of an accurately "calibrated" method of cascade analysis. At increased bombarding energy, the method developed here should therefore allow to identify internal conversion in the continuum region. As explained in Sec. I, one expects to be especially sensitive to the lowest-energy transitions and thus to be able to extend studies on this subject carried out by electron spectroscopy.[14]

We would like to point out that the general form we have given to our cascade analysis permits the algorithm to be used also for other than nuclear cascades where two deexcitation mechanisms compete.

Note added in proof. After this paper was submitted for publication, work using similar methods appeared in the literature: H. J. Karwowski, S. E. Vigdor, W. W. Jacobs, S. Kailas, P. P. Singh, F. Soga, and W. D. Ploughe, Phys. Rev. Lett. 42, 1732 (1979); and Z. Sujkowski, D. Chmielewska, R. V. F. Janssens, and M. J. A. de Voigt, Phys. Rev. Lett. 43, 998 (1979).

ACKNOWLEDGMENTS

We are indebted to O. W. B. Schult and to V. Zoran for discussions, and to T. Rose for help in the preparation of some of the figures. This work was supported in part by the Bundesministerium für Forschung und Technologie, Bonn, West Germany.

APPENDIX: CASCADE ANALYSIS

We formulate a procedure which allows the evaluation of the individual $S_f^i(\text{calc})$ for an arbitrary choice of the transition γ_f^i in the cascade of the residual nucleus.

A. Arbitrary cascade

We introduce two probabilities in order to break up $S_f^i(\text{calc})$ into its constituents.

(i) To describe the level *populations* throughout the cascade we remember that the levels are numbered in order of increasing excitation energy, with number 0 for the ground state. We call P_{nm} the probability that a cascade path passing through a given level n has passed through a level m above n, or will pass through a level m below n. This implies, of course, that $P_{nn}=1$. We will discuss the calculation of the P_{nm} for a given nuclear cascade below. We only note that of course many of the P_{nm} vanish, since the various cascade paths, in general, involve only part of the levels.

(ii) We express by $X(\rightarrow f)$ the probability that the transitions populating level f produce a nuclear-satellite K *x ray* by internal conversion. We have

$$X(\rightarrow f)\equiv\sum_{i>f}{}^{s}I_f^i(\alpha_K)_f^i\omega_K/F(f)\,. \tag{A1}$$

The quantity $F(f)$ is the *total feeding* of level f by both cascade and side feeding:

$$F(f)\equiv\sum_{i>f}A_f^i+F_s(f)\,,$$

where also, (A2)

$$F(f)\equiv\sum_{j<f}A_j^f\,,\quad \text{for } f>0\,.$$

Here, $F_s(f)$ is the side feeding of level f. In an analogous way, the probability for x-ray production by the transitions starting in level i is

$$X(i\rightarrow)\equiv\sum_{j<i}{}^{s}I_j^i\,(\alpha_K)_j^i\omega_K/F(i)\,,\quad \text{for } i>0\,. \tag{A3}$$

With the definitions (A1)–(A3) we are able to express the summed probability for x-ray emission coincident with transition $i\rightarrow f$, $S_f^i(\text{calc})$, in a condensed way:

$$S_f^i(\text{calc})=\sum_{m=i}^{N}X(\rightarrow m)P_{im}+\sum_{m=1}^{f}X(m\rightarrow)P_{fm}\,. \tag{A4}$$

Before $S_f^i(\text{calc})$ can be evaluated according to this equation we have to construct explicit expressions for the P_{nm} of the population matrix. This requires an analysis of the cascade paths.

We proceed in a recursive way, starting at the diagonal, for which

$$P_{mm}=1\,,\quad \text{for all } m\geq 0\,. \tag{A5a}$$

Suppose now the elements P_{nm} of column m *above* the diagonal ($n<m$) to be known until $P_{n+1,m}$. Then the next-higher element P_{nm} is given by the following considerations: all cascade paths connecting level m with level $n+1$ are already taken into account by $P_{n+1,m}$. Proceeding to level n below $n+1$ in the cascade brings into play the additional transition intensities $A_n^{n+1},A_n^{n+2},\ldots,A_n^m$, some or all of which might be zero, depending on the specific case of decaying nucleus. The contribution of the intermediate level $n+k$ ($1\leq k\leq m-n$) to P_{nm} is the probability, $A_n^{n+k}/F(n)$, that the population of level n starts from level $n+k$, multiplied by the probability that a cascade path through level $n+k$ has passed through level m, i.e., $P_{n+k,m}$. After summation over the intermediate levels $n+k$ this yields

$$P_{nm}=\sum_{k=1}^{m-n}\frac{A_n^{n+k}}{F(n)}P_{n+k,m}\,,\quad \text{for } n<m,\ \text{all } m>0\,. \tag{A5b}$$

Since P_{0m} does not occur in Eq. (A4), the need to actually construct it according to Eq. (A5b) and to obtain $F(0)$ from (A2) does not arise.

The P_{nm} *below* the diagonal are related to those above the diagonal by the relation

$$P_{nm}=[F(m)/F(n)]P_{mn}\,,\quad \text{for } n>m\,,\ \text{all } n>0\,. \tag{A5c}$$

This is easily seen, since the intensity of the cascade paths leading through both level n and level m can be expressed in two ways: (i) the intensity of the paths through m that have previously passed through n, $F(m)P_{mn}$; and (ii) the intensity of the paths through n that subsequently pass through m, below, i.e., $F(n)P_{nm}$. The equality of these two expressions yields Eq. (A5c).

With Eqs. (A5) the construction of the P_{nm} is complete for an arbitrary cascade, and $S_f^i(\text{calc})$ can be evaluated according to Eq. (A4).

B. Special case

We want to use the special case that only ground-state transitions are considered to show how Eqs. (A4) and (A5) work. We will thereby rederive the simple procedure of Eq. (7) in Sec. V. We proceed by evaluating the first part of Eq. (7), i.e., the quantity

$$\xi_K^{\text{calc}}\equiv\sum_{n=1}^{N}S_0^n(\text{calc})A_0^n\,,$$

by using our expressions (A4) and (A5) for the $S_0^n(\text{calc})$. We have from Eqs. (7) and (A4)

$$\sum_{n=1}^{N}A_0^nS_0^n(\text{calc})=\sum_{n=1}^{N}\left(A_0^n\sum_{m=n}^{N}X(\rightarrow m)P_{nm}\right),$$

where N is the highest of the levels for which there is a γ decay known. The double sum can be rearranged to yield

$$\sum_{n=1}^{N} A_0^n S_0^n(\text{calc}) = \sum_{m=1}^{N} X(\rightarrow m) \sum_{n=1}^{m} A_0^n P_{nm} . \qquad \text{(A6)}$$

The sum over n is then rewritten by using the relations

$$A_0^1 = F(1), \quad A_0^n = F(n) - \sum_{k=1}^{n-1} A_k^n, \quad \text{for } n > 1,$$

and Eqs. (A5):

$$\begin{aligned}
\sum_{n=1}^{m} A_0^n P_{nm} &= \sum_{n=1}^{m} F(n) P_{nm} - \sum_{n=2}^{m} \sum_{k=1}^{n-1} A_k^n P_{nm} \\
&= F(m) + \sum_{n=1}^{m-1} \sum_{k=1}^{m-n} A_n^{n+k} P_{n+k,m} - \sum_{n=2}^{m} \sum_{k=1}^{n-1} A_k^n P_{nm} \\
&= F(m) + \sum_{n=1}^{m-1} \sum_{k=n+1}^{m} A_n^k P_{km} - \sum_{n=2}^{m} \sum_{k=1}^{n-1} A_k^n P_{nm} \\
&= F(m) + \sum_{k=2}^{m} \sum_{n=1}^{k-1} A_n^k P_{km} - \sum_{n=2}^{m} \sum_{k=1}^{n-1} A_k^n P_{nm} \\
&= F(m) .
\end{aligned}$$

With this identity we rewrite Eq. (A6) as

$$\begin{aligned}
\sum_{n=1}^{N} A_0^n S_0^n(\text{calc}) &= \sum_{m=1}^{N} X(\rightarrow m) F(m) \\
&= \sum_{m=1}^{N} \sum_{i>m} {}^{s}I_m^i (\alpha_K)_m^i \omega_K ,
\end{aligned}$$

where we have used expression (A1) for $X(\rightarrow m)$. The double sum is running just over all identified transitions of the whole cascade, except those leading to the ground level, $m = 0$. Thus we finally have

$$\sum_{n=1}^{N} A_0^n S_0^n(\text{calc}) = \sum_{\substack{i,m \\ m \neq 0}} {}^{s}I_m^i (\alpha_K)_m^i \omega_K ,$$

which is Eq. (7) of Sec. V. Our general cascade analysis thus contains the more direct approach of Eq. (7) as a special case.

[1] C. H. Rutledge and R. L. Watson, At. Data Nucl. Data Tables 12, 195 (1973).

[2] E. Laegsgaard, J. U. Andersen, and M. Lund, in *Proceedings of the Tenth International Conference on the Physics of Electronic and Atomic Collisions, Paris, 1977*, edited by G. Watel (North-Holland, Amsterdam, 1978), p. 353.

[3] M. Dost, S. Hoppenau, J. Kising, S. Röhl, and W. A. Schönfeldt, in *Abstracts of the Tenth International Conference on the Physics of Electronic and Atomic Collisions, Paris, 1977* (Commissariat à l'Energie Atomique, Paris, 1977), p. 72.

[4] R. Anholt, Phys. Rev. A 17, 983 (1978).

[5] T. L. Hardt and R. L. Watson, Phys. Rev. A 7, 1917 (1973).

[6] A. W. Waltner, D. M. Peterson, G. A. Bissinger, A. B. Bashkin, C. E. Busch, P. H. Nettles, W. R. Scates, and S. M. Shafroth, in *Proceedings of the International Conference on Inner Shell Ionization Phenomena and Future Applications, Atlanta, 1972*, edited by R. W. Fink *et al.*, (Oak Ridge, U. S. Atomic Energy Commission, 1972), p. 1080.

[7] G. Deconninck and N. Longequeue, Phys. Rev. Lett. 30, 863 (1973).

[8] G. Deconninck, G. Demortier, and F. Bodart, At. Energy Rev. 13, 367 (1975).

[9] S. Röhl, S. Hoppenau, M. Dost, and H. J. Stein, *Proceedings of the International Symposium on Nuclear Structure, Balatonfüred, Hungary, 1975*, edited by I. Fodor-Lovas and G. Palla (Készült a Központi Fizikai Kutató Intézet, Budapest, 1976), Vol. 2, p. 365.

[10] G. Deconninck and M. Longrée, Phys. Rev. A 16, 1390 (1977).

[11] C. P. Randell, J. S. C. McKee, and S. F. J. Wilk, J. Phys. G 2, L69 (1976); Nucl. Instrum. Methods 142, 33 (1977).

[12] A. Berinde, C. Deberth, I. Neamu, C. Protop, N. Scintei, V. Zoran, M. Dost, and S. Röhl, J. Phys. B 11, 2875 (1978).

[13] H. Seyfarth, N. Wüst, and O. W. B. Schult, Z. Phys. A 280, 239 (1977).

[14] S. J. Feenstra, W. J. Ockels, J. Van Klinken, M. J. A. De Voigt, and Z. Sujkowski, Phys. Lett. B 69, 403 (1977).

[15] W. de Wieclawik, C. R. Acad. Sci. B 266, 577 (1968).

[16] R. J. Walen, C. Briançon, and M. Valadares, in Ref. 6, p. 1906.

[17] V. Metag, D. Habs, H. J. Specht, G. Ulfert, and C. Kozhuharov, Hyperfine Interactions 1, 405 (1976).

[18] J. Sau, A. Demeyer, and R. Chéry, Nucl. Phys. A 121, 131 (1968).

[19] N. E. Scott, J. W. Cobble, and P. J. Daly, Nucl. Phys. A 119, 131 (1968).

[20] D. Vinciguerra, K. Kotajima, and R. E. Van de Vijver, Nucl. Phys. 77, 337 (1966).

[21] H. E. Kurz, E. W. Jaspers, K. Fischer, and F. Hermes, Nucl. Phys. A 168, 129 (1971).

[22] A. R. Barnett and J. S. Lilley, Phys. Rev. C 9, 2010 (1974).

[23] W. John, Jr., Phys. Rev. 103, 704 (1956).

[24] W. J. Ramler, J. Wing, D. J. Henderson, and J. R. Huizenga, Phys. Rev. 114, 154 (1959).

[25] K. A. Keller, J. Lange, and H. Münzel, in *Landoldt-Börnstein, Zahlenwerte und Funktionen aus Naturwissenschaft und Technik*, edited by H. Schopper (Springer-Verlag, Berlin, 1974), Vol. I 5c.

[26] G. Winter, L. Funke, K. Hohmuth, K. H. Kaun, P. Kemnitz, and H. Sodan, Nucl. Phys. A 151, 337

(1970).
[27]P. Kemnitz, L. Funke, K. H. Kaun, H. Sodan, W. Winter, and M. I. Baznat, Nucl. Phys. A 209, 271 (1973).
[28]P. P. Singh, L. J. Medsker, G. T. Emery, L. A. Beach, and C. R. Gosset, Phys. Rev. C 10, 656 (1974).
[29]*Nuclear Level Schemes A=45 through A=257*, edited by Nuclear Data Group (Academic, New York, 1973).
[30]L. Bergström, J. Blomqvist, C. J. Herrlander, and K. Wikström, Phys. Scr. 10, 292 (1974).
[31]J. Bergström, J. Blomqvist, C. J. Herrlander, K. Wikström, and B. Fant, Phys. Scr. 10, 287 (1974).
[32]B. Fant, Phys. Scr. 4, 175 (1971).
[33]G. Astner, Phys. Scr. 5, 31 (1972).
[34]W. Bambynek, B. Crasemann, R. W. Fink, H. U. Freund, H. Mark, C. D. Swift, R. E. Price, and P. Venugopala Rao, Rev. Mod. Phys. 44, 716 (1972).
[35]J. O. Newton, Phys. Rev. 117, 1520 (1960).
[36]C. W. Lewis, R. L. Watson, and J. B. Natowitz, Phys. Rev. A 5, 1773 (1972).
[37]R. S. Hager and E. C. Seltzer, in *Atomic and Nuclear Data Reprints*, edited by K. Way (Academic, London, 1973), p. 1.
[38]M. T. Lu and W. P. Alford, Phys. Rev. C 3, 1243 (1971).
[39]B. Harmatz and T. H. Handley, Nucl. Phys. A 121, 481 (1968).
[40]V. Zoran, A. Berinde, C. Deberth, M. Dost, I. Neamu, C. Protop, S. Röhl, and N. Scintei, J. Phys. G (in press).